RSC Medicinal Chemistry

ROYAL SOCIETY OF CHEMISTRY

RESEARCH ARTICLE

View Article Online
View Journal | View Issue

Cite this: *RSC Med. Chem.*, 2025, **16**, 4837

Site-dependent modulation of antitumor activity and fluorescence in thieno[3,2-*b*]pyridin-5(4*H*)-ones†

Dan-Bi Sung, [ab] Pham Van Thong,[ac] Jieun Yun,[d] Joo-Hee Kwon,[d] Sol Park,[a] Sang Kook Woo, [b] Jong Soon Kang [d] and Jong Seok Lee *[ac]

We report the design and synthesis of thieno[3,2-*b*]pyridin-5(4*H*)-one derivatives exhibiting site-dependent modulation of both antitumor activity and fluorescence, enabled by a regioselective BOP-promoted aza-[3 + 3] cycloaddition. The reaction proceeds between thiophen-3-amines and α,β-unsaturated carboxylic acids, followed by base-induced dehydrogenation. Mechanistic studies reveal that the head-to-tail aza-[3 + 3] annulation involves a *C*-1,4 conjugate addition, leading to an intramolecular amide coupling. Evaluation of the photophysical properties and antitumor activities demonstrated that the biological and optical behaviours of the thieno[3,2-*b*]pyridin-5(4*H*)-one scaffold are dependent on the aryl substitution site. Specifically, 3-aryl derivatives exhibited notable antitumor activity, whereas 2-aryl analogues displayed strong fluorescence, highlighting the potential of this scaffold for dual-function applications. DFT calculations supported the observed divergence in fluorescence by revealing differences in orbital conjugation and HOMO–LUMO gaps. In addition, selected compounds showed low cytotoxicity toward MRC-9 cells, indicating favourable cancer cell selectivity.

Received 8th May 2025,
Accepted 11th July 2025

DOI: 10.1039/d5md00399g

rsc.li/medchem

Introduction

Cycloaddition reactions represent powerful, convergent strategies for the construction of structurally complex carbocyclic and heterocyclic scaffolds.[1] Owing to their efficiency in forming multiple bonds with defined regio- and stereochemistry, substantial efforts have focused on developing both concerted and stepwise cycloaddition reactions with high selectivity. Among these, the aza-[3 + 3] cycloaddition has emerged as a particularly versatile approach for assembling nitrogen-containing six-membered heterocycles, including pyridines, pyridinones, and piperidines—core motifs frequently encountered in natural products and pharmacologically active compounds.[2–4] Unlike traditional pericyclic reactions, these transformations are more accurately described as formal [3 + 3] cycloadditions, proceeding through stepwise mechanisms involving two fragments with complementary reactivity. Based on the connectivity pattern of newly formed bonds within the piperidine ring system, these annulations can be further classified into two mechanistic types (Fig. 1A, a).[2]

Type 1 cycloadditions involve bond formation at the C2–C3 and C5–C6 positions, a mode characteristic of double Mannich-type reactions, while type 2 cycloadditions proceed *via* N–C2 and C4–C5 bond formation, often observed in reactions involving iminium ions or aziridines as electrophiles. Additionally, the concept of regioselectivity—specifically, the distinction between 'head-to-head' and 'head-to-tail' annulation—adds a further layer of refinement to the classification framework.[3] In 'head-to-head' processes, the electrophilic and nucleophilic termini of both fragments engage symmetrically, typically furnishing 1,2-dihydropyridine scaffolds *via* terminal–terminal bond formation. Conversely, 'head-to-tail' annulations proceed through crosswise bond formation between asymmetric termini, most commonly *via* Cβ–N bond formation followed by intramolecular cyclization, leading to distinct ring topologies and substitution patterns (Fig. 1A, b).

Achieving precise regioselective control in aza-[3 + 3] cycloadditions remains a key synthetic challenge, with undesired isomeric mixtures often arising from competing pathways (Fig. 1B). For instance, Hsung's protocol using vinylogous amides and α,β-unsaturated iminium salts reliably

[a] *Marine Natural Products Chemistry Laboratory, Korea Institute of Ocean Science & Technology (KIOST), Busan 49111, Republic of Korea. E-mail: jslee@kiost.ac.kr*
[b] *Department of Chemistry, Pusan National University, Busan 46241, Republic of Korea*
[c] *Department of Marine Technology & Convergence Engineering, Korea University of Science and Technology, Daejeon 34113, Republic of Korea*
[d] *Laboratory Animal Resource Center, Korea Research Institute of Bioscience and Biotechnology, Cheongju 28116, Republic of Korea*

† Electronic supplementary information (ESI) available: Full experimental procedures, characterization, ^{1}H-, ^{13}C-NMR spectra of the new compounds. See DOI: https://doi.org/10.1039/d5md00399g

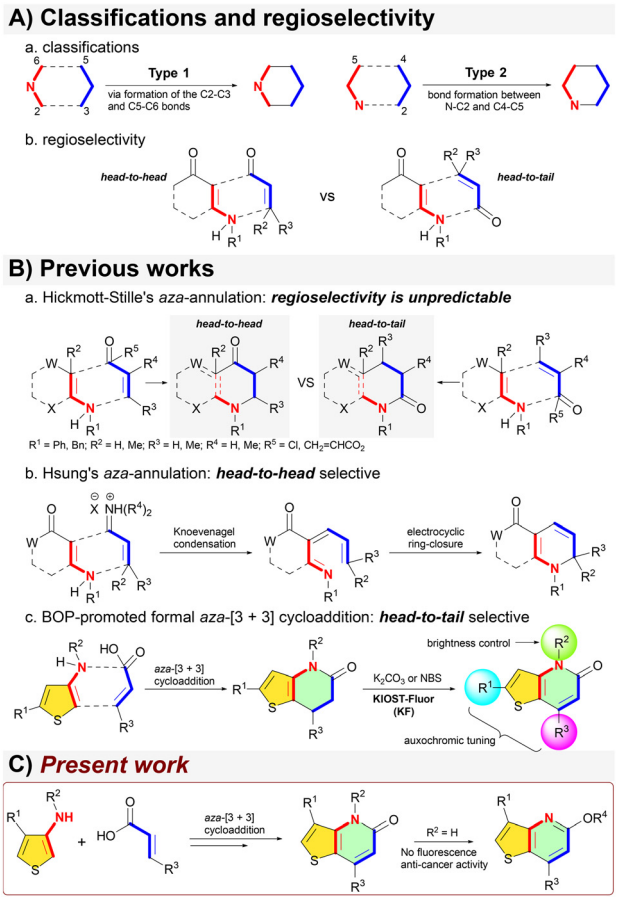

Fig. 1 BOP-promoted formal aza-[3 + 3] cycloaddition reaction.

yields 'head-to-head' products with excellent selectivity,[5–14] whereas Hickmott–Stille-type annulations involving acid anhydrides or chlorides often result in regioisomeric mixtures due to ambiguous alignment of reactive sites.[15–19]

In our recent work, we reported the regioselective synthesis of 2-arylthieno[3,2-*b*]pyridin-5(4*H*)-ones (designated **KIOST-Fluor**, **KF**) *via* a BOP (benzotriazol-1-yloxytris(dimethylamino) phosphonium hexafluorophosphate)-promoted aza-[3 + 3] cycloaddition between 3-amino-5-arylthiophenes and α,β-unsaturated carboxylic acids (Fig. 1B, c).[20] These compounds displayed strong fluorescence, with emission wavelengths spanning 426–678 nm in dichloromethane and 424–610 nm in acetonitrile, accompanied by large Stokes shifts and high quantum yields.

As part of our ongoing efforts to probe the structure–property relationships of the thieno[3,2-*b*]pyridin-5(4*H*)-one scaffold and further elucidate the mechanism of BOP-promoted annulation, we expanded the substrate scope and investigated a new series of 3-aryl-substituted derivatives (Fig. 1C).[21–23] Herein, we report the synthesis and characterization of these compounds, examine their photophysical and antitumor properties, and highlight a striking example of site-dependent functional divergence, demonstrating the dual potential of this scaffold for biomedical and optical applications.

Results and discussion

Chemistry

The synthetic route toward the target thieno[3,2-*b*]pyridine derivatives commenced with the preparation of 3-arylthiophen-4-amines (**6**) *via* a five-step sequence (Scheme 1). Bromination of commercially available 3-aminothiophene **1** using $Ph(Me)_3NBr_3$ and $CaCO_3$ in a MeOH/DCM (methanol/dichloromethane) mixture at rt (room temperature) afforded the corresponding 2-bromo intermediate **2**,[24] which was hydrolysed under basic conditions (1 N KOH) to yield the carboxylic acid **3**. Subsequent silica gel-promoted decarboxylation of the carboxylic acid **3** in EtOAc (ethyl acetate)/MeOH provided 4-bromothiophene-3-amine **4**, which underwent a Suzuki–Miyaura cross-coupling reaction with arylboronic acids in the presence of $Pd(PPh_3)_4$ and Na_2CO_3 in refluxing toluene to furnish corresponding 4-arylthiophene-3-amines **5**.[25] Furthermore, a methyl group was introduced to the amino group of **5b** and **5e** with NaH and MeI affording **6a** and **6b** in good yields. The core thieno[3,2-*b*]pyridin-5(4*H*)-one framework was assembled *via* a BOP-promoted aza-[3 + 3] annulation between 4-arylthiophen-3-amines (**5** and **6**) and α,β-unsaturated carboxylic acids in the presence of DIPEA (*N*,*N*-diisopropylethylamine) and DMF (*N*,*N*-dimethylformamide), followed by base-induced dehydrogenation to yield the final products (**10** and **11**) (Scheme 2). The annulation proceeds *via* a 'head-to-tail' regioselective pathway, featuring a tandem sequence of *C*-1,4 conjugate addition, followed by intramolecular *N*-1,2-addition (amide bond formation) and subsequent aromatization under basic conditions (Fig. 2). Mechanistic insights were gained through the isolation of compound **8** as the major product and compound **9** as a minor side product of the aza-[3 + 3] cycloaddition. The formation of compound **9** is consistent with an initial *N*-1,2-addition; however, its inability to undergo the subsequent intramolecular *C*-1,4 conjugate addition suggests that this reverse sequence is not favoured under the reaction conditions.

These observations support the proposed stepwise mechanism in which *C*-1,4 addition precedes *N*-1,2 cyclization, thereby facilitating efficient annulation and

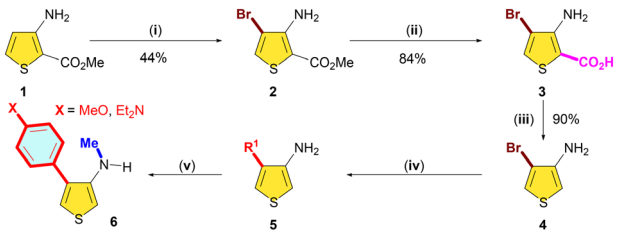

5a: R^1 = Ph (86%); **5b**: R^1 = 4-MeO-Ph (90%); **5c**: R^1 = 4-CF_3O-Ph (83%); **5d**: R^1 =4-Ph-Ph 72%); **5e**: R^1 = 4-Et_2N-Ph (99%); **5f**: R^1 = 4-(Piperidin-1-yl)-Ph (52%); **5g**: R^1 = Furan-2-yl (58%); **5h**: R^1 = Thiophen-2-yl (66% brsm); **5i**: R^1 = 3,4,5-tri(MeO)-Ph (99%); **5j**: R^1 = 4-(Pyrrolidin-1-yl)-Ph (84%); **6a**: X = MeO (40%); **6b**: X = Et_2N (59%)

Scheme 1 Synthesis of 3-arylthiophen-4-amines **5** and **6**. (i) $Ph(Me)_3NBr_3$, $CaCO_3$, MeOH/DCM; (ii) 1 N KOH; (iii) silica gel, EtOAc/MeOH; (iv) $Pd(PPh_3)_4$, boronic acids, Na_2CO_3, toluene, reflux; (v) NaH, MeI, DMF, rt.

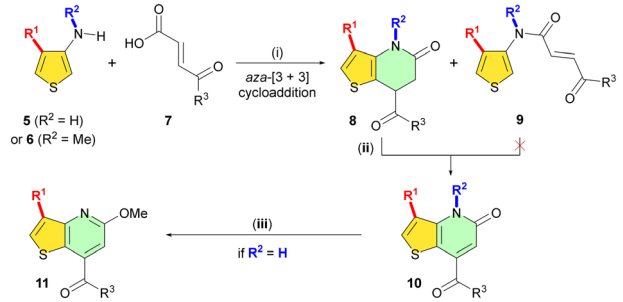

Scheme 2 Synthesis of thieno[3,2-*b*]pyridine derivatives **10** and **11**. (i) BOP, DIPEA, DMF, rt; (ii) K_2CO_3, DMF, rt; (iii) MeI, K_2CO_3, DMF, 0 °C to rt.

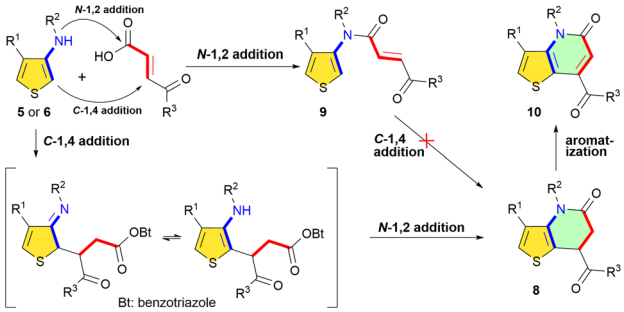

Fig. 2 Proposed mechanism of the BOP-promoted aza-[3 + 3] cycloaddition.

successful construction of the thieno[3,2-*b*]pyridin-5(4*H*)-one framework (Fig. 2). This modular strategy enabled rapid access to a structurally diverse library of thieno[3,2-*b*]pyridine derivatives suitable for further biological and photophysical evaluation.

Photophysical properties

We first examined the photophysical profiles of the synthesized thieno[3,2-*b*]pyridine-5(4*H*)-one derivatives in dichloromethane (10 μM), using the previously reported 2-aryl analogues as a reference standard. According to our earlier findings, 2-arylthieno[3,2-*b*]pyridin-5(4*H*)-ones (**KF** series) displayed strong fluorescence with high quantum yields (Φ_F up to 0.99), large Stokes shifts (up to 232 nm), and bathochromically tunable emission maxima in the visible range. Electron-rich substituents (*e.g.*, methoxy, phenoxy, or *N*,*N*-dialkylamino groups) at the *para*-position of the C2-aryl ring substantially enhanced fluorescence intensity and red-shifted emission wavelengths, suggesting efficient π-conjugation across the heterocyclic core. The photophysical properties of representative compounds **KF-2**, **KF-22**, **10bb**, and **10eo** are summarized in Table 1. Notably, both **KF-2** and **KF-22** exhibited strong fluorescence, with high quantum yields of 90% and 91%, respectively. In contrast, compound **10bb** displayed a measurable emission at 446 nm upon excitation at 371 nm, but with a quantum yield of 0%, indicating highly inefficient radiative decay. Compound **10eo** did not exhibit detectable emission under the tested conditions, and its quantum yield could not be determined.

This stark contrast in the photophysical properties highlights a regioisomeric divergence: C2 substitution permits π-conjugation between the aryl moiety and the electron-deficient pyridone core, whereas C3 substitution likely perturbs the orbital overlap or introduces non-radiative decay pathways. As shown in Fig. 3, the underlying synthetic divergence between the two regioisomeric series also reflects a mechanistic distinction: while 2-aryl derivatives arise from C2-arylated thiophen-3-amines, the current work utilizes C3-arylated analogues as the aza-[3 + 3] cycloaddition partners. This seemingly subtle difference results in a distinct electronic topology of the final thieno[3,2-*b*]pyridin-5(4*H*)-one core, which likely accounts for the fluorescence quenching observed in the 3-aryl series. The synthetic framework in Fig. 3 thereby helps rationalize the observed site-dependent photophysical behaviour.

The density functional theory (DFT) and time-dependent (TD)-DFT results clearly elucidate the distinct fluorescence behaviours of **10bb**, **10eo**, **KF-2**, and **KF-22** (Fig. 4, see Section S4 of ESI† for details). The 2-aryl-substituted compounds **KF-2** and **KF-22** benefit from extended π-conjugation between the aryl ring and the thieno[3,2-*b*]pyridin-5(4*H*)-one core, whereas the 3-aryl-substituted analogues **10bb** and **10eo** lack such conjugation due to significant steric repulsion between the 3-aryl group and the adjacent *N*-methyl substituent, leading to electronic decoupling. This structural difference is reflected in the orbital energy diagram: **KF-22** possesses the highest occupied molecular orbital (HOMO) energy (−5.34 eV) and the narrowest HOMO–lowest unoccupied molecular orbital (LUMO) gap (2.86 eV), while **10bb** shows the lowest HOMO level (−6.22 eV) and the widest gap (3.74 eV) (Fig. 4). These trends are consistent with their oscillator strengths, with **KF-22** showing the highest value (f = 0.6359), followed

Table 1 Photophysical properties of 2-aryl- and 3-arylthieno[3,2-*b*]pyridine-5(4*H*)-ones[a]

Compd.	Absorbance (λ_{abs})	Excitation (λ_{ex})	Emission (λ_{em})	Quantum yield (%)
KF-2[b]	400	412	472	90
KF-22[b]	442	463	562	91
10bb	235	371	446	0
10eo	283	0	0	—

[a] Absorbance, excitation, emission, and absolute quantum yield at 10 μM in CH_2Cl_2. [b] Data from ref. 20.

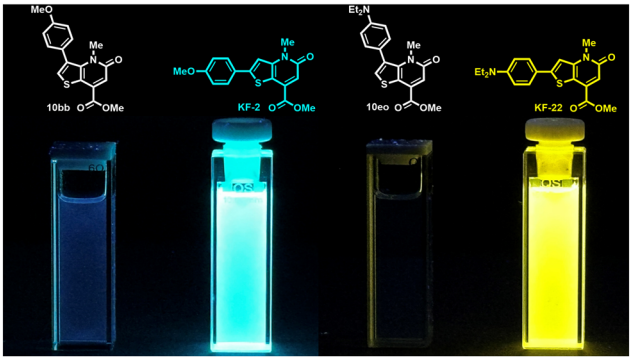

Fig. 3 Fluorescence comparison of 2-aryl and 3-arylthieno[3,2-*b*]pyridin-5(4*H*)-ones (10 μM in CH_2Cl_2, excited at 365 nm under a UV lamp).

by **KF-2** (f = 0.5356), **10eo** (f = 0.1827), and **10bb** (f = 0.1087) (see Section S4 of ESI† for details). The strong oscillator strengths of the 2-aryl compounds reflect efficient orbital overlap and enhanced transition dipole moments, resulting in bright fluorescence. In contrast, the lower oscillator strengths of **10bb** and **10eo** are indicative of poor conjugation and diminished radiative efficiency. These differences underscore the critical role of molecular planarity and substitution pattern in tuning photophysical properties.

Overall, the combination of narrowed energy gaps, elevated HOMO levels, and strong oscillator strengths explains the superior fluorescence of **KF-2** and **KF-22**. These results demonstrate the site-dependent functional differentiation of the thieno[3,2-*b*]pyridine-5(4*H*)-ones: the 2-aryl series serves as a promising platform for tunable fluorescent probes, while the 3-aryl analogues, though non-emissive, are anticipated to exhibit distinct biological activities, further supporting the dual utility of this framework in both photonic and pharmacological applications.

Antitumor activity

To evaluate the anticancer potential of the synthesized 3-arylthieno[3,2-*b*]pyridin-5(4*H*)-ones, a series of compound **10** analogues was tested against six human cancer cell lines: ACHN (renal), MDA-MB-231 (breast), HCT-15 (colon), NUGC-3 (gastric), PC-3 (prostate), and NCI-H23 (lung).[26] Growth inhibition was quantified by GI_{50} values, defined as the concentration required to reduce cell proliferation by 50% (Table 2, see Section S5 of ESI† for details). In addition, cytotoxicity against the normal human lung fibroblast cell line MRC-9 was evaluated to assess selectivity.

Several analogues bearing electron-donating groups at the *para*-position of the C3-aryl ring (R^1) exhibited notable cytotoxicity, with GI_{50} values below 20 μM in at least one cell line. Among them, compound **10i**, bearing a 3,4,5-trimethoxyphenyl group at R^1, demonstrated consistently

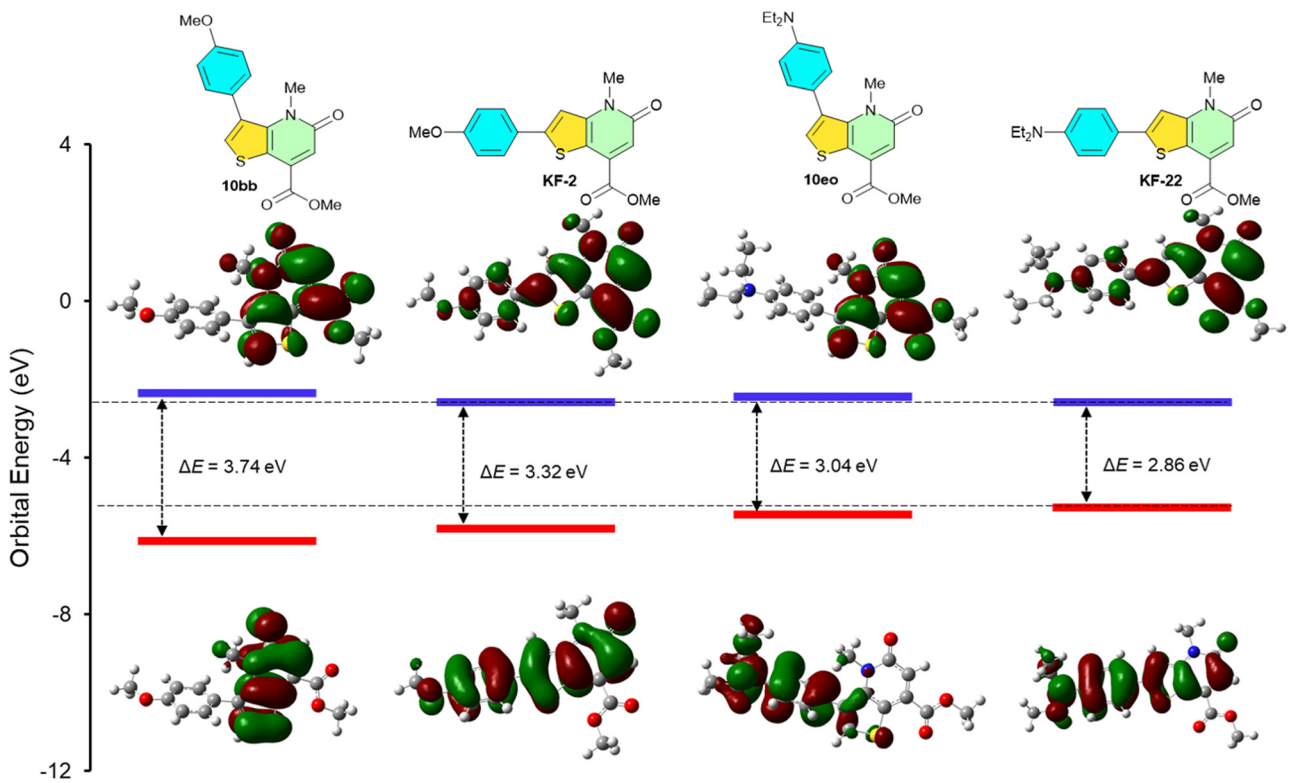

Fig. 4 Comparative representation of calculated HOMO–LUMO energy levels (eV) and electron density distributions in HOMO–LUMO for aryl-substituted thieno[3,2-*b*]pyridin-5(4*H*)-one derivatives. Calculations were performed at the B3LYP/6-311+G(d)/CPCM(dichloromethane) level of theory.

Table 2 Growth inhibitory activities (GI_{50}) of compound **10** analogues in six human cancer cell lines[a]

Substituents[b]

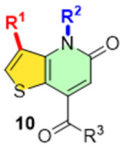

Compd.	R^1	R^2	R^3	Human cancer cell lines (GI_{50})[c] ACHN	MDA-MB-231	HCT-15	NUGC-3	PC-3	NCI-H23	MRC-9
10a	Ph	H	OMe	105.1	105.1	105.1	105.1	105.1	105.1	35.4
10ba	4-MeO-Ph	H		95.1	95.1	95.1	95.1	95.1	95.1	67.1
10bb		Me		13.2	14.3	18.4	15.8	11.7	12.0	90.1
10c	4-CF_3O-Ph	H		81.2	81.2	81.2	81.2	81.2	81.2	81.2
10d	4-Ph-Ph	H		83.0	83.0	83.0	83.0	83.0	83.0	35.3
10ea	4-Et_2N-Ph	H	OMe	16.2	20.4	26.3	24.0	15.5	21.7	24.1
10eb		H	Ph	74.5	74.5	74.5	74.5	74.5	74.5	74.5
10ec		H	4-Me-Ph	16.8	22.2	18.1	13.3	18.2	16.9	30.8
10ed		H	4-MeO-Ph	15.9	16.1	16.5	13.4	17.6	14.1	18.7
10ee		H	3-MeO-Ph	50.7	45.3	44.2	33.2	41.0	36.5	58.1
10ef		H	2-MeO-Ph	16.5	20.8	15.6	15.1	17.8	15.8	24.8
10eg		H	3,4-Methylenedioxy-Ph	67.2	67.2	67.2	67.2	67.2	67.2	67.2
10eh		H	4-Ph-Ph	62.7	62.7	62.7	62.7	62.7	62.7	62.7
10ei		H	4-EtO-Ph	67.2	67.2	67.2	67.2	67.2	67.2	67.2
10ej		H	4-PhO-Ph	27.8	23.6	37.0	27.5	31.7	31.4	40.3
10ek		H	2,5-di-MeO-Ph	64.9	64.9	64.9	64.9	64.9	64.9	64.9
10el		H	3,4-di-MeO-Ph	50.0	32.9	41.9	26.0	33.5	44.1	46.9
10em		H	2-Furanyl	49.4	45.8	45.5	38.7	37.3	48.4	60.2
10en		H	Cyclopropyl	19.3	22.7	27.5	18.9	16.9	23.0	51.8
10eo		Me	OMe	81.0	81.0	81.0	81.0	81.0	81.0	25.8
10f	4-(Piperidin-1-yl)-Ph	H	OMe	81.4	81.4	81.4	81.4	81.4	81.4	81.4
10g	2-Furanyl			109.0	109.0	109.0	109.0	109.0	109.0	109.0
10h	2-Thiophenyl			58.4	63.3	64.0	53.1	51.1	55.8	79.8
10i	3,4,5-tri-MeO-Ph			10.2	12.3	9.6	12.7	21.5	9.0	25.4
10j	4-(Pyrrolidin-1-yl)-Ph			84.6	84.6	84.6	84.6	84.6	84.6	84.6

[a] GI_{50} values represent the mean of at least two independent experiments and are reported in μM. [b] R^1 = C3-aryl substituent; R^2 = *N*-substituent; R^3 = substituent of the ketone or ester moiety. [c] ACHN: renal carcinoma; MDA-MB-231: breast carcinoma; HCT-15: colon carcinoma; NUGC-3: gastric carcinoma; PC-3: prostate carcinoma; NCI-H23: lung carcinoma; MRC-9: lung fibroblast.

strong activity across all six cell lines (GI_{50} = 9.0–21.5 μM), and maintained a reasonable selectivity margin with an MRC-9 GI_{50} of 25.4 μM. Likewise, compound **10bb**, featuring a 4-methoxyphenyl group at R^1 and an *N*-methyl substituent at R^2, showed potent and uniform cytotoxicity (GI_{50} = 11.7–18.4 μM), while demonstrating low toxicity to normal cells (MRC-9 GI_{50} = 90.1 μM), suggesting a favourable combination of electronic and steric effects as well as high selectivity. Substituent effects at R^3 were also evident. Analogues with *para*-substituted aryl groups bearing electron-donating functionalities, such as **10ec** (4-Me) and **10ed** (4-MeO), displayed enhanced cytotoxicity, with GI_{50} values below 20 μM across most tested cell lines, while still maintaining moderate selectivity (MRC-9 GI_{50} = 30.8 and 18.7 μM, respectively). These results suggest that favourable electronics and substitution patterns at R^3 can overcome potential steric bulk while maintaining selectivity.

In contrast, *ortho*- or *meta*-substituted analogues such as **10ee** (3-MeO) and **10ef** (2-MeO) showed more variable activity, likely due to suboptimal orientation or diminished conjugation with the core scaffold, and exhibited moderate cytotoxicity in MRC-9 (GI_{50} = 58.1 μM and 24.8 μM, respectively). Substitution at R^2 (the nitrogen atom) also modulated activity in selected cases. For example, *N*-methylation (as in **10bb** and **10eo**) may influence lipophilicity or conformational preference. However, **10eo**, despite having similar R^1 and R^2 features to **10bb**, showed markedly reduced activity (GI_{50} > 80 μM), although it retained low toxicity in MRC-9 (GI_{50} = 25.8 μM), indicating that the electronic character of R^1 is a dominant factor in determining potency. Compounds bearing bulky or rigid substituents at R^1, such as **10d** (biphenyl), showed poor activity (GI_{50} > 80 μM), likely due to steric hindrance disrupting productive molecular interactions, and also showed limited selectivity (MRC-9 GI_{50} = 35.3 μM). Similarly, bulk at R^3 was unfavourable in **10eh**, where a biphenyl substituent at R^3 diminished potency despite an electron-rich diethylaminophenyl group at R^1. Additionally, electron-deficient substituents at R^1, such as the 4-trifluoromethoxyphenyl group in **10c**, were associated with weak activity, reinforcing the SAR trend that electron-rich R^1 groups are more favourable for cytotoxicity. Taken together, compounds with electron-rich, *para*-substituted aryl groups at either R^1 (*e.g.*, **10j**, **10bb**) or R^3 (*e.g.*, **10ec**, **10ed**) exhibited

enhanced cytotoxicity while maintaining acceptable selectivity, supporting the conclusion that favourable electronic properties and substitution patterns at both positions promote target engagement. These enhancements may arise from improved π-stacking, hydrogen bonding, or optimal spatial orientation within a binding pocket. Interestingly, compound **10en**, which lacks an R^1 substituent and features a compact, non-aromatic cyclopropyl group at R^3, demonstrated consistent moderate activity across all six cell lines (GI_{50} = 16.9–27.5 μM), and showed moderate toxicity in MRC-9 (GI_{50} = 51.8 μM) (Table 2).

This observation suggests that, beyond electronics, conformationally restricted and hydrophobic groups at R^3 may also contribute to cytotoxicity by enabling shape complementarity or enhancing membrane permeability.

We next evaluated a second series of compounds (compound **11** analogues), which differ from the **10** series primarily by variation at R^1 and R^3, with R^2 fixed as hydrogen. GI_{50} values for this series across the same six cancer cell lines are presented in Table 3. Several analogues in the **11** series showed promising activity. Compound **11el**, bearing a 3,4-dimethoxyphenyl group at R^3, exhibited sub-20 μM activity across most cell lines (GI_{50} = 11.6–15.4 μM) and low toxicity in MRC-9 (GI_{50} = 17.8 μM). Likewise, compound **11ej**, featuring a 4-phenoxyphenyl group at R^3, also displayed favourable potency (GI_{50} = 13.8–21.3 μM) with an MRC-9 GI_{50} of 28.0 μM. The most potent analogue in the series was compound **11f**, which possesses a 4-(piperidin-1-yl)phenyl group at R^1 and a methoxy group at R^3. It achieved GI_{50} values between 5.6 and 8.7 μM, indicating that basic heterocyclic groups at R^1 can significantly enhance cytotoxicity, likely by improving solubility, membrane permeability, or specific target binding. Importantly, **11f** exhibited high selectivity, with a much weaker effect on MRC-9 cells (GI_{50} = 78.4 μM).

In contrast, analogues bearing electron-withdrawing or sterically bulky groups at R^3, such as **11c** (4-CF_3O-Ph), **11d** (biphenyl), and **11h** (2-thiophenyl), exhibited poor or negligible activity (GI_{50} > 80 μM), and were generally less selective. Similarly, *ortho*-substituted aryl groups at R^3, exemplified by **11ef** (2-MeO), were associated with reduced potency (GI_{50} = 67.2 μM) and moderate toxicity in MRC-9 (GI_{50} = 67.2 μM), likely due to steric hindrance or misalignment with the pharmacophore. The observed variation in cytotoxicity is attributable to differences in R^1 and R^3. Among these, the electronic and steric features of R^3 emerged as primary determinants of activity, while electron-rich or basic substituents at R^1—such as in **11f**—also contributed significantly to potency.

Taken together, the compound **11** series reinforces the SAR trends established in the **10** series: electron-rich, *para*-substituted aryl groups and compact, basic heterocycles at R^1 or R^3 are most favourable for anticancer activity. These substituent patterns are proposed to enhance target engagement through π-stacking, hydrogen bonding, and

Table 3 Growth inhibitory activities (GI_{50}) of compound **11** analogues in six human cancer cell lines[a]

Substituents[b]

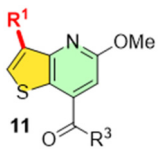

Compd.	R^1	R^3	Human cancer cell Lines[c] ACHN	MDA-MB-231	HCT-15	NUGC-3	PC-3	NCI-H23	MRC-9
11a	Ph	OMe	100.2	100.2	100.2	100.2	100.2	100.2	46.3
11b	4-MeO-Ph		39.5	50.8	49.6	45.4	32.6	27.3	102.6
11c	4-CF_3O-Ph		78.3	78.3	78.3	78.3	78.3	78.3	27.8
11d	4-Ph-Ph		79.9	79.9	79.9	79.9	79.9	79.9	79.9
11ea	4-Et_2N-Ph	OMe	81.0	81.0	81.0	81.0	81.0	81.0	41.2
11eb		Ph	46.5	47.0	38.1	41.2	48.1	40.0	48.7
11ec		4-Me-Ph	45.6	42.7	37.9	33.9	45.4	47.0	43.6
11ed		4-MeO-Ph	34.6	32.8	36.5	42.9	41.5	45.4	54.3
11ee		3-MeO-Ph	40.9	41.8	30.7	42.6	40.1	49.2	71.4
11ef		2-MeO-Ph	67.2	67.2	67.2	67.2	67.2	67.2	67.2
11eg		3,4-Methylenedioxy-Ph	65.1	65.1	65.1	65.1	65.1	65.1	65.1
11eh		4-Ph-Ph	10.9	13.5	8.8	6.7	10.1	12.3	16.6
11ei		4-EtO-Ph	65.1	65.1	65.1	65.1	65.1	65.1	65.1
11ej		4-PhO-Ph	15.5	21.3	15.5	13.8	13.8	21.0	28.0
11ek		2,5-di-MeO-Ph	62.9	62.9	62.9	62.9	62.9	62.9	62.9
11el		3,4-di-MeO-Ph	11.8	15.4	14.0	12.2	11.6	14.0	17.8
11em		2-Furanyl	45.5	48.4	40.1	43.3	42.2	41.6	48.7
11en		Cyclopropyl	52.1	52.9	43.7	55.8	39.8	51.8	50.7
11f	4-(Piperidin-1-yl)-Ph	OMe	8.7	5.6	7.1	8.4	7.4	6.7	78.4
11g	2-Furanyl		103.7	103.7	103.7	103.7	103.7	103.7	103.7
11h	2-Thiophenyl		98.2	98.2	98.2	98.2	98.2	98.2	98.2

[a] GI_{50} values represent the mean of at least two independent experiments and are reported in μM. [b] R^1 = C3-aryl substituent; R^3 = substituent of the ketone or ester moiety. [c] Cell line abbreviations as described in Table 2.

favourable spatial alignment within the binding pocket, while MRC-9 data further support that several lead compounds, including **10bb** and **11f**, exhibit promising selectivity profiles for future development.

Conclusions

We have developed a modular, regioselective approach to access a structurally diverse library of 3-aryl-substituted thieno[3,2-*b*]pyridin-5(4*H*)-ones through a BOP-promoted aza-[3 + 3] cycloaddition, followed by base-mediated aromatization. This methodology complements our previously reported synthesis of 2-aryl analogues and enables direct comparisons of site-dependent functional behaviour within a unified heterocyclic scaffold. Mechanistic studies, including the isolation of key intermediates (compounds **8** and **9**), support a stepwise annulation mechanism proceeding through initial *C*-1,4 conjugate addition followed by *N*-1,2 addition. The failure of the reverse pathway—initiating with *N*-1,2 addition—to yield the annulated product reinforces the mechanistic preference and efficiency of the *C*-1,4-first sequence (Fig. 2).

Photophysical characterization revealed a striking divergence in fluorescence behaviour between the two regioisomeric series: while 2-aryl derivatives exhibited strong and tunable fluorescence with high quantum yields, 3-aryl analogues displayed negligible emission. This divergence is attributed to differences in electronic topology and π-conjugation pathways arising from the site of aryl substitution on the thieno[3,2-*b*]pyridin-5(4*H*)-one scaffold. These findings were further supported by DFT and TD-DFT calculations, which provided insights into orbital distributions, energy levels, and oscillator strengths.

Biological evaluations demonstrated that several 3-aryl analogues—particularly those bearing *para*-electron-donating or heterocyclic substituents—exhibited moderate to potent cytotoxicity across multiple cancer cell lines, with GI_{50} values in the low micromolar range. Notably, some of the most active compounds, such as **10i** and **11f**, reached sub-10 μM potency, indicating promising anticancer potential. Evaluation of cytotoxicity against the normal lung fibroblast cell line MRC-9 further enabled an assessment of selectivity, revealing that compounds such as **10bb** and **11f** displayed favourable therapeutic indices.

Together, these findings underscore the significance of regioselective design in tailoring molecular properties. The thieno[3,2-*b*]pyridin-5(4*H*)-one scaffold offers a dual-function platform: C2-aryl substitution favours photonic applications, while C3-aryl substitution enables pharmacological optimization. This site-dependent divergence highlights the potential of this scaffold for multifunctional applications in both medicinal chemistry and materials science.

Data availability

The data supporting this article have been included as part of the ESI.†

Author contributions

DBS, SP, and PVT carried out the chemical synthesis under the supervision of SKW and JSL. DBS conducted the photophysical property measurements supervised by JSL. JY and JHK performed the cancer cell growth inhibition assays under the supervision of JSK. The manuscript was drafted by DBS and JSL and reviewed by all authors.

Conflicts of interest

There are no conflicts to declare.

Acknowledgements

This work was supported by KIOST (PEA0311), Republic of Korea.

Notes and references

1 S. Kobayashi and K. A. Jorgensen, *Cycloaddition Reactions in Organic Synthesis*, Wiley-VCH Verlag GmbH & Co, KGaA, 2002.
2 J. P. A. Harrity and O. Provoost, *Org. Biomol. Chem.*, 2005, **3**, 1349–1358.
3 S. B. Grant, B. F. John and P. H. Richard, *Curr. Org. Synth.*, 2010, **7**, 363–401.
4 J. Deng, X.-N. Wang and R. P. Hsung, *Methods and Applications of Cycloaddition Reactions in Organic Syntheses*, 2014, pp. 283–354.
5 R. P. Hsung, L.-L. Wei, H. M. Sklenicka, C. J. Douglas, M. J. McLaughlin, J. A. Mulder and L. J. Yao, *Org. Lett.*, 1999, **1**, 509–512.
6 R. P. Hsung, H. C. Shen, C. J. Douglas, C. D. Morgan, S. J. Degen and L. J. Yao, *J. Org. Chem.*, 1999, **64**, 690–691.
7 L.-L. Wei, R. P. Hsung, H. M. Sklenicka and A. I. Gerasyuto, *Angew. Chem., Int. Ed.*, 2001, **40**, 1516–1518.
8 H. M. Sklenicka, R. P. Hsung, M. J. McLaughlin, L.-L. Wei, A. I. Gerasyuto and W. B. Brennessel, *J. Am. Chem. Soc.*, 2002, **124**, 10435–10442.
9 M. J. McLaughlin, R. P. Hsung, K. P. Cole, J. M. Hahn and J. Wang, *Org. Lett.*, 2002, **4**, 2017–2020.
10 S. Luo, C. A. Zificsak and R. P. Hsung, *Org. Lett.*, 2003, **5**, 4709–4712.
11 N. Sydorenko, R. P. Hsung, O. S. Darwish, J. M. Hahn and J. Liu, *J. Org. Chem.*, 2004, **69**, 6732–6738.
12 N. Sydorenko, C. A. Zificsak, A. I. Gerasyuto and R. P. Hsung, *Org. Biomol. Chem.*, 2005, **3**, 2140–2144.
13 A. I. Gerasyuto, R. P. Hsung, N. Sydorenko and B. Slafer, *J. Org. Chem.*, 2005, **70**, 4248–4256.
14 G. S. Buchanan, H. Dai, R. P. Hsung, A. I. Gerasyuto and C. M. Scheinebeck, *Org. Lett.*, 2011, **13**, 4402–4405.
15 P. W. Hickmott and G. Sheppard, *J. Chem. Soc. C*, 1971, 1358–1362.
16 K. Paulvannan and J. R. Stille, *J. Org. Chem.*, 1992, **57**, 5319–5328.

17 K. Paulvannan, J. B. Schwarz and J. R. Stille, *Tetrahedron Lett.*, 1993, **34**, 215–218.
18 K. Paulvannan and J. R. Stille, *Tetrahedron Lett.*, 1993, **34**, 6673–6676.
19 P. Benovsky, G. A. Stephenson and J. R. Stille, *J. Am. Chem. Soc.*, 1998, **120**, 2493–2500.
20 D.-B. Sung, B. Mun, S. Park, H.-S. Lee, J. Lee, Y.-J. Lee, H. J. Shin and J. S. Lee, *J. Org. Chem.*, 2019, **84**, 379–391.
21 S. Lee, D.-B. Sung, S. Kang, S. Parameswaran, J.-H. Choi, J. S. Lee and M. S. Han, *Sensors*, 2019, **19**, 5298.
22 S. Lee, D.-B. Sung, J. S. Lee and M. S. Han, *ACS Omega*, 2020, **5**, 32507–32514.
23 D.-B. Sung, J. H. Han, Y.-K. Kim, B. H. Mun, S. Park, H. S. Kim and J. S. Lee, *J. Org. Chem.*, 2022, **87**, 4936–4950.
24 K. Tateno, K. Ono and H. Kawai, *Chem. – Eur. J.*, 2019, **25**, 15765–15771.
25 N. Matuszak, G. G. Muccioli, G. Labar and D. M. Lambert, *J. Med. Chem.*, 2009, **52**, 7410–7420.
26 H. J. Shin, S.-Y. Jung, J. S. Kang, C.-S. Heo and S. J. Park, *J. Nat. Prod.*, 2024, **87**, 2432–2440.

